Determination of the Two-Dimensional Interaction Rate Constants of a Cytokine Receptor Complex

Martynas Gavutis, Eva Jaks, Peter Lamken, and Jacob Piehler
Institute of Biochemistry, Johann Wolfgang Goethe-University, Frankfurt, Germany

ABSTRACT Ligand-receptor interactions within the plane of the plasma membrane play a pivotal role for transmembrane signaling. The biophysical principles of protein-protein interactions on lipid bilayers, though, have hardly been experimentally addressed. We have dissected the interactions involved in ternary complex formation by ligand-induced cross-linking of the subunits of the type I interferon (IFN) receptors ifnar1 and ifnar2 in vitro. The extracellular domains ifnar1-ectodomain (EC) and ifnar2-EC were tethered in an oriented manner on solid-supported lipid bilayers. The interactions of IFNα2 and several mutants, which exhibit different association and dissociation rate constants toward ifnar1-EC and ifnar2-EC, were monitored by simultaneous label-free detection and surface-sensitive fluorescence spectroscopy. Surface dissociation rate constants were determined by measuring ligand exchange kinetics, and by measuring receptor exchange on the surface by fluorescence resonance energy transfer. Strikingly, approximately three-times lower dissociation rate constants were observed for both receptor subunits compared to the dissociation in solution. Based on these directly determined surface-dissociation rate constants, the surface-association rate constants were assessed by probing ligand dissociation at different relative surface concentrations of the receptor subunits. In contrast to the interaction in solution, the association rate constants depended on the orientation of the receptor components. Furthermore, the large differences in association kinetics observed in solution were not detectable on the surface. Based on these results, the key roles of orientation and lateral diffusion on the kinetics of protein interactions in plane of the membrane are discussed.

INTRODUCTION

Protein-protein interactions within the plane of cellular membranes play a key role for many biological processes and in particular for transmembrane signaling. These lateral interactions are not static and are typically triggered or stabilized by interactions with further interaction partners such as ligands, effectors, and binding proteins from the matrices adjacent to the lipid bilayers. A prominent example is the ligand-induced cross-linking of receptor tyrosine kinases (1,2) and cytokine receptors (3), where two-dimensional interaction between receptor subunits have been recognized to be important for regulating signaling (4–7). The fundamental importance of such coupled interactions for cell-surface receptor activation has stimulated numerous theoretical studies (8–13). The underlying concept of these models is the reduction in dimensionality upon ligand binding to a membrane-anchored receptor (14). The binding of ligands to individual surface receptors can be determined by standard techniques, and rate constants and equilibrium constants are measured in the same units as for interaction in solution. In the second step, however, lateral interactions take place in the plane of the membrane, i.e., in two instead of three space dimensions. For several reasons, the kinetic parameters of these interactions cannot be readily deduced from the rate constants of the same interaction in solution:

1. Anchoring of the proteins into the membrane reduces the translational and rotational freedom, and results in a preferred orientation of the interaction partners to each other along the normal of the surface. Hence, the reaction diagram and the reaction coordinate of the interaction are different from the interaction in solution.
2. Lateral and rotational diffusion of the membrane-anchored protein is much slower than in solution, while the dynamics of the amino-acid side chains mediating the interaction between the proteins are not affected.

The consequences of these constraints have been subject of numerous speculations and theoretical consideration, but to date only very few semiquantitative (4) or quantitative (15,16) experimental approaches toward characterizing two-dimensional interactions on membranes have been reported.

Recently, we have reported an experimental approach for reconstituting and analyzing membrane-anchored proteins on solid-supported lipid bilayers (17). The extracellular receptor domains of the type I interferon (IFN) receptor subunits ifnar1 (ifnar1-ectodomain, EC) and ifnar2 (ifnar2-EC) were tethered in an oriented manner onto solid-supported lipid bilayers providing well-defined and homogeneous diffusion kinetics (18). The interaction of the membrane-anchored receptor subunits with the ligand IFNα2 was studied by using simultaneous surface-sensitive fluorescence and interference detection (19). This approach enables to monitor and vary the concentrations of the receptor subunits

Submitted August 12, 2005, and accepted for publication January 4, 2006.

Address reprint requests to Jacob Piehler, Institute of Biochemistry, Biocenter N210, Johann Wolfgang Goethe-University, Marie-Curie-Strasse 9, 60439 Frankfurt am Main, Germany. Tel.: 49-0-69-7982-9468; E-mail: j.piehler@em.uni-frankfurt.de.

Abbreviations used: ifnar, type I interferon receptor; H10, decahistidine-tag; tl, tag-less.

© 2006 by the Biophysical Society

0006-3495/06/05/3345/11 $2.00

doi: 10.1529/biophysj.105.072546

on the lipid bilayer, and the absolute surface concentrations can be quantified. A rigorous analysis of all possible interactions between the three partners established ternary complex formation by independent interaction of ifnar1 and ifnar2 with the ligand IFNα2 (18,19). A general mechanism describing the two possible pathways of ternary complex formation and dissociation is depicted in Fig. 1. Altogether, four separate interactions have to be considered: two of them (described by K_1 and K_4) involve ligand binding from solution to the surface receptor subunits. The affinity of IFNα2 toward ifnar2-EC (K_1: 5 nM) is approximately three orders-of-magnitude higher than the affinity toward ifnar1-EC (K_4: $\sim$5 μM) (18). In contrast, the interactions of the binary complexes on the surface with the second receptor subunits (described by K_2 and K_3) are two-dimensional interactions. Despite its inherent three-body complexity, several striking features make this interaction a particularly suitable system for studying surface interactions: First, the receptor subunits independently interact from each other with the ligand, and do not interact with each other as proposed for other cytokine receptors. Second, only a heterodimeric ternary complex was detectably involving ifnar2-EC, ifnar1-EC, and IFNα2 in a 1:1:1 stoichiometry. Thus, the surface interaction is triggered by a ligand binding from solution and the equilibria K_2 and K_3 between binary and ternary complex on the surface K_2 and K_3 can be probed by the dissociation kinetics of the ligand from the surface (19). Since receptor surface concentrations can be absolutely quantified in the reconstituted system, this provides the means for determining the equilibrium dissociation constants of these two-dimensional interactions.

Because ligand binding to ifnar2-EC (k_1) is at least 10-times faster than to ifnar1-EC (k_4), pathway 1 has been assumed to be substantially favored both for formation and for the dissociation of the ternary complex at stoichiometric surface concentrations of the receptor subunits. For an IFNα2 mutant with reduced k_1, however, pathway 2 has been proposed to considerably contribute, which may hold true also for other members of the type I IFN family (19). Here, we have employed the features of this system to explore the biophysical principles governing protein interactions in plane of biological membranes. By using different chasing and pulse-chasing assays, as well as IFN-mutants with different affinities and different association and dissociation rate constants of the interaction with ifnar1-EC and ifnar2-EC, each of the two-dimensional rate constants of the two interaction pathway depicted in Fig. 1 were determined. Furthermore, the role of electrostatic rate enhancement and the relative orientation of the receptor subunits on the surface-association rate constants were investigated. Based on these data, we compare the determinants of protein interaction kinetics in three and two dimensions.

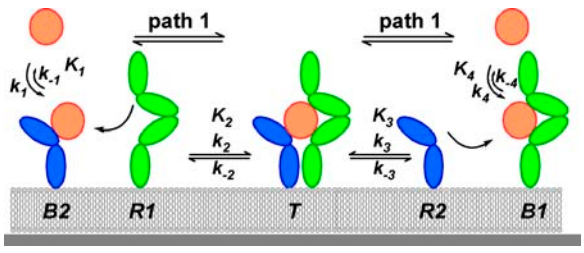

FIGURE 1 Schematic of the dynamic equilibria of solution and surface interactions involved in the two-step formation and dissociation of the ternary IFN-receptor complex on a membrane (details in the text).

MATERIALS AND METHODS

Protein expression and purification

IFNα2, IFNα2 HEQ, ifnar2-EC with a C-terminal decahistidine-tag (ifnar2-H10), ifnar2-H10 I47A, and tag-less ifnar2-EC (ifnar2-tl) were expressed in *Escherichia coli*, refolded from inclusion bodies and purified by anion-exchange and size-exclusion chromatography as described (20). For site-specific labeling, an additional cysteine was introduced by the mutations S136C (IFNα2) and S35C (ifnar2-H10). These proteins were expressed, refolded, and purified as the wild-type proteins. After size-exclusion chromatography, these proteins were incubated with a threefold excess of Alexa Fluor 488 (AF488) maleimide or Oregon Green 488 (OG488) maleimide as fluorescence resonance energy transfer (FRET) donors, and Alexa Fluor 568 (AF568) maleimide as an FRET acceptor (all from Molecular Probes, Eugene, OR). After the labeling reaction, the proteins were further purified by anion exchange chromatography. Binding experiments confirmed that the interaction properties of both proteins were not affected by mutagenesis or labeling. Ifnar1-EC with a C-terminal decahistidine tag (Ifnar1-H10) and with an N-terminal decahistidine tag (H10-ifnar1) were expressed in Sf9 insect cells, and purified from the supernatant by immobilized metal-affinity chromatography followed by size-exclusion chromatography as described earlier (21).

Simultaneous fluorescence interference detection

Two-dimensional interactions were detected with a homebuilt setup for simultaneous reflectance interferometry (RIf) and total internal reflection fluorescence spectroscopy (TIRFS) detection as described previously in more detail (19). An argon ion laser was used for fluorescence excitation at 488 nm at an excitation power of 2–3 μW focused onto an area of 1 mm^2 to minimize photobleaching. Fluorescence was collected by an optical fiber and detected by a photomultiplier tube through bandpass filters. FRET measurements with donor and acceptor fluorescence detection were carried out by changing the emission filters by means of a filter wheel. Mass deposition onto the surface was monitored simultaneously by RIf detection at 800 nm. Both TIRFS and RIf were acquired with a time resolution of 1.2–1.5 s. Sample handling was carried out in a flowthrough format using a syringe pump as described (22). With this system, flow rates between 1 and 500 μl/s can be employed. Sample handling and data acquisition were controlled with software written in LabVIEW (National Instruments, Austin, TX).

Lipid bilayer assembling, receptor reconstitution, and binding assays

The transducer surface was incubated for 30 min in a freshly prepared mixture of two-parts 30% (v/v) hydrogen peroxide and three-parts concentrated sulfuric acid. After extensive washing with water, the transducer was dried in a nitrogen stream and mounted immediately into the flow cell. Solid supported lipid bilayers were prepared by fusion of small unilamellar vesicles obtained by probe sonication. Synthetic stearoyl-oleoyl phosphatidylcholine (Avanti Polar Lipids, Alabaster, AL) lipids were doped

with 5 mol % lipid containing *bis*-NTA chelator head (19). The unsaturated alkyl chain of both matrix and chelator lipid prevented phase segregation and ensured bilayer fluidity.

All binding studies were carried out with 20 mM HEPES, pH 7.5, and 150 mM NaCl as the running buffer at a temperature of 25°C. Solid-supported lipid bilayers were obtained by injecting small unilamellar vesicles at a lipid concentration of 250 μM on the surface of the transducer. Protein immobilization and binding assays were in principle carried out as described earlier (18). For tethering the histidine-tagged proteins to the supported membranes, the chelator headgroups were loaded with Ni^{2+} ions by injecting 10 mM nickel(II)chloride in the running buffer for 150 s and conditioned by a 150 s injection of 200 mM imidazole. Depending on the targeted surface concentrations, the his-tagged proteins were sequentially injected at concentrations between 2 nM and 1 μM for 20–60 s. The ligand was then injected at a concentration of 50 nM for 150–300 s with a flow rate of 1 μl/s. Spontaneous dissociation was monitored either by washing with HBS at a flow rate of 10 μl/s or by injection of 2 μM ifnar2-tl to suppress rebinding due to the high association rate constant of IFNα2 toward ifnar2-EC. This concentration of ifnar2-tl was determined experimentally to be sufficient at all receptor surface concentrations employed in this study, and is in line with theoretical considerations according to Goldstein et al. (23). For ligand-chasing experiments, 1 μM IFNα2 or 1 μM IFNα2 HEQ were injected at a flow rate of 1 μl/s for 300–450 s. For pulse-chase experiments, 1 μM ifnar2-H10 was injected for 20 s, followed by a buffer wash with a flow rate of 10 μl/s. After a set of ligand-binding experiments, all attached proteins were removed by a 150 s pulse of 200 mM imidazole, and the subsequent binding assays were carried out on the same lipid bilayer.

Data evaluation

Binding curves were analyzed using Origin (Microcal Software, Northampton, MA) or Berkeley Madonna (UCB, Berkeley, CA) software packages. If necessary, RIf curves were corrected for a linear drift based on the signals before tethering the proteins and after regeneration with imidazole. Two different models were used to evaluate ligand dissociation curves. Dissociation rate constants were obtained by fitting a monoexponential function:

$$R(t) = R_0 \times e^{-k_d \cdot (t - t_0)}. \quad (1)$$

Two-dimensional association rate constants were determined by fitting a two-step dissociation model describing one of the two pathways shown in Fig. 1 as in principle described before (19). For determination of k_2 (pathway 1), the following set of differential equations was fitted:

$$\begin{aligned}\frac{d[T]}{dt} &= k_2 \times [B2] \times ([R1]_0 - [T]) - k_{-2} \times [T]\\ \frac{d[B2]}{dt} &= -k_2 \times [B2] \times ([R1]_0 - [T]) + k_{-2} \times [T] - k_{-1} \times [B2]\\ [S] &= [T] + [B2], \quad \text{with} \quad T_{t=0} = [R1]_0, [B2]_{t=0} = 0. \quad (2)\end{aligned}$$

$[B2] = 0$ was assumed as initial conditions because $[T] \gg [B]$. Owing to the fast fluctuation between T and B2 ($\sim 1\ s^{-1}$) compared to the ligand dissociation kinetics, the true values of [B2] and [T] are reached very quickly during numerical integration (19).

For determination of k_3 (pathway 2), the following set of differential equations was fitted:

$$\begin{aligned}\frac{d[T]}{dt} &= k_3 \times [B1] \times ([R2]_0 - [T]) - k_{-3} \times [T]\\ \frac{d[B1]}{dt} &= -k_3 \times [B1] \times ([R2]_0 - [T]) + k_{-3} \times [T] - k_{-4} \times [B1]\\ [S] &= [T] + [B1], \quad \text{with} \quad T_{t=0} = [R2]_0, [B1]_{t=0} = 0. \quad (3)\end{aligned}$$

$[B1] = 0$ can be assumed as initial condition for the same reason given above. $[R1]_0$ and $[R2]_0$ were initial surface concentrations of ifnar1-EC and ifnar2-EC, respectively, which were determined from the RIf signals. The value [S] was the total surface concentration of the ligand, which was detected in a time-resolved manner by the TIRFS signal and converted into an absolute surface concentration using a calibration by RIf. The two-dimensional dissociation rate constants k_{-2} and k_{-3}, respectively, were determined independently by chasing experiments. The respective two-dimensional association rate constant was the only parameter varied in the fitting procedure.

Simulations

Ligand dissociation kinetics through both pathways was numerically simulated using the set of differential equations

$$\begin{aligned}\frac{d[T]}{dt} &= k_2 \times [B2] \times ([R1]_0 - [T] - [B1]) - k_{-2} \times [T]\\ &\quad + k_3 \times ([B1] \times ([R2]_0 - [T] - [B2]) - k_{-3} \times [T])\\ \frac{d[B2]}{dt} &= -k_2 \times [B2] \times ([R1]_0 - [T] - [B1])\\ &\quad + k_{-2} \times [T] - k_{-1} \times [B2]\\ \frac{d[B1]}{dt} &= -k_3 \times [B1] \times ([R2]_0 - [T] - [B2])\\ &\quad + k_{-3} \times [T] - k_{-4} \times [B1]\\ \frac{d[path1]}{dt} &= -k_{-1} \times [B2], \frac{d[path2]}{dt} = -k_{-4} \times [B1]\\ [S] &= [T] + [B2] + [B1]\\ [S] &= [path1] + [path2], \quad (4)\end{aligned}$$

where [path1] and [path2] represent the concentrations of the ligand dissociating through path 1 and path 2, respectively. During the simulation, the same initial conditions were used as for fitting experimental curves: $[T]_{t=0} = 2\ fmol/mm^2, [B2]_{t=0} = 0, [B1]_{t=0} = 0$. $[R1]_0$ and $[R2]_0$ were parameterized to be 2 or 22 $fmol/mm^2$. Before plotting [S], [path1] and [path2] were normalized to $[T]_{t=0}$.

RESULTS

The interaction kinetics of ifnar2-EC and ifnar1-EC with IFNα2 has been previously studied in detail, and numerous mutants with different interaction rate constants have been described (18,24–27). Here, we used several mutants of IFNα2 and ifnar2-EC, as well as different variants of ifnar1-EC. The rate constants of the mutants applied for further characterization of the two-dimensional interaction involved in ternary complex formation were verified by ligand binding assays with the site-specifically fluorescence-labeled IFNα2 species using TIRFS detection (Table 1).

Pathways of receptor assembling and dissociation

IFN-induced two-step assembling and dissociation of the ternary complex with ifnar1-EC and ifnar2-EC can occur by two different pathways (Fig. 1). For the interaction of IFNα2 with ifnar2-EC and ifnar1-EC at stoichiometric concentration, pathway 1 has been considered to determine both complex formation and dissociation, because of the faster association

TABLE 1 Parameters of the individual interactions between IFNα2 and the receptor subunits

	Ifnar2-H10			Ifnar2-H10 I47A			Ifnar1-H10/H10-ifnar1		
IFNα2	k_a (k_1) [M^{-1} s^{-1}]	k_d (k_{-1}) [s^{-1}]	K_D (K_1) nM	k_a (k_1) [M^{-1} s^{-1}]	k_d (k_{-1}) [s^{-1}]	K_D (K_1) nM	k_a (k_4) [M^{-1} s^{-1}]	k_d (k_{-4}) [s^{-1}]	K_D (K_4) nM
wt	3×10^6	0.02	7	3×10^6	0.4	150	2×10^5	1	5000
R144A	3×10^5	0.044	150	3×10^5	0.5	1700	2×10^5	1	5000
HEQ	3×10^6	0.02	7	3×10^6	0.2	70	2×10^5	0.05	250

In brackets, the identifier of the constants as introduced in Fig. 1 are given. All IFNα2 species were site-specifically fluorescence-labeled with OG488 or AF488 by incorporating the additional mutation S136C.

rate constant k_1 compared to k_4 (19). This holds obviously true for the complex formation, since ligand binding from solution is the rate-limiting step of the assembling process (19), which is ~10-fold faster to ifnar2-EC than to ifnar1-EC. Dissociation of the ternary complex, however, is determined by the two-dimensional rate constants k_2, k_{-2}, k_3, and k_{-3}, which have been assumed to scale relatively as the corresponding rate constants in solution. This assumption was qualitatively tested by rapidly changing the receptor surface concentration after formation of a stoichiometric ternary complex (Fig. 2). Ifnar1-EC and ifnar2-EC carrying a C-terminal decahistidine-tag (ifnar1-H10 and ifnar2-H10) were site-specifically tethered in stoichiometric concentrations onto silica-supported lipid bilayers doped with *bis*-NTA lipids. The dissociation kinetics of fluorescence-labeled IFNα2 (^{AF488}IFNα2) was monitored before and after tethering additional ifnar1-H10 onto the membrane (Fig. 2, *B* and *C*). As expected, slower ligand dissociation kinetics was observed upon loading additional ifnar1-H10, indicating a shift of the equilibrium K_2 toward the ternary complex (see Fig. 1). Surprisingly, however, a similar effect was observed when the ifnar2-H10 surface concentration was rapidly increased under the same conditions (Fig. 2, *D* and *E*). An approximately twofold-higher molar surface concentration of ifnar2-EC compared to ifnar1-EC in the previous experiment was required to obtain similar dissociation kinetics. However, since only pathway 2 depends on the surface concentration of ifnar2, this result indicates that this pathway is significantly involved in the dissociation of the ternary complex. Properly describing the receptor dynamics therefore requires dissection of all four two-dimensional rate constants involved in ternary complex formation.

Two-dimensional dissociation kinetics measured by FRET

The dissociation rate constant of the two-dimensional interaction between ifnar2-H10 and the IFNα2 complexed by ifnar1-H10 was directly measured using a pulse-chase approach, which is schematically depicted in Fig. 3 *A*. After ternary complex formation of ^{AF568}IFNα2 with ^{AF488}ifnar2-H10 and ifnar1-H10, a substantial excess of unlabeled ifnar2-H10 was rapidly tethered onto the membrane, and the exchange of ^{AF488}ifnar2-H10 from ternary complex with unlabeled ifnar2-H10 was monitored by the decaying FRET between ^{AF568}IFNα2 and ^{AF488}ifnar2-H10. A typical experiment is shown in Fig. 3 *B*. Donor fluorescence from ^{AF488}ifnar2-H10 was quenched upon ternary complex formation with acceptor-labeled ^{AF568}IFNα2, which was accompanied by an increase in sensitized fluorescence. During rinsing, slow recovery of the donor fluorescence and likewise decay of the acceptor fluorescence due to ligand dissociation was observed. Upon pulse-chasing the ternary complex by rapidly tethering an ~10-fold excess of unlabeled ifnar2-H10 onto the membrane, much faster recovery of the donor fluorescence and decay of the acceptor fluorescence were observed. Under these conditions, ligand dissociation was hardly detectable (Figs. 2 *D* and 3 *C*), confirming that indeed the kinetics of the exchange of ^{AF488}ifnar2-H10 against unlabeled ifnar2-H10 on the surface was monitored by FRET. The normalized traces for donor and acceptor fluorescence were in excellent agreement (Fig. 3 *C*). Because of the high excess of unlabeled ifnar2-EC on the surface, the rate constant of this exchange is determined by the two-dimensional dissociation rate constant of the ifnar2-H10/IFNα2 complex k_{-3}, which is the rate-limiting step in this process. The rate constants obtained by a mono-exponential fit to the two FRET signals were in good agreement and an average k_{-3} of 0.007 ± 0.001 s^{-1} was determined from multiple experiments at different receptor surface concentrations. Strikingly, k_{-3} is approximately three-times lower than the k_{-1} of 0.02 s^{-1} for the dissociation of IFNα2 from ifnar2-H10 into solution (see Fig. 3 *C* and Table 1). Extensive ligand binding studies with the receptor domains in solution have excluded that the interactions of the receptor subunits with IFNα2 affect each other through conformational changes imposed on the ligand or direct contacts between the receptor subunits. Thus, the difference between k_{-1} and k_{-3} results from anchoring the complex onto the membrane.

Determination of two-dimensional rate constants by ligand chasing

To confirm this effect on the dissociation kinetics, the two-dimensional dissociation rate constants were assessed by ligand-chasing experiments. The principle of this assay is depicted in Fig. 4 *A*. Here, a high excess of ifnar1-EC compared to ifnar2-H10 was tethered onto the membrane, and the ternary complex was formed by injecting ^{AF488}IFNα2. The excess of ifnar1-H10 remained free due

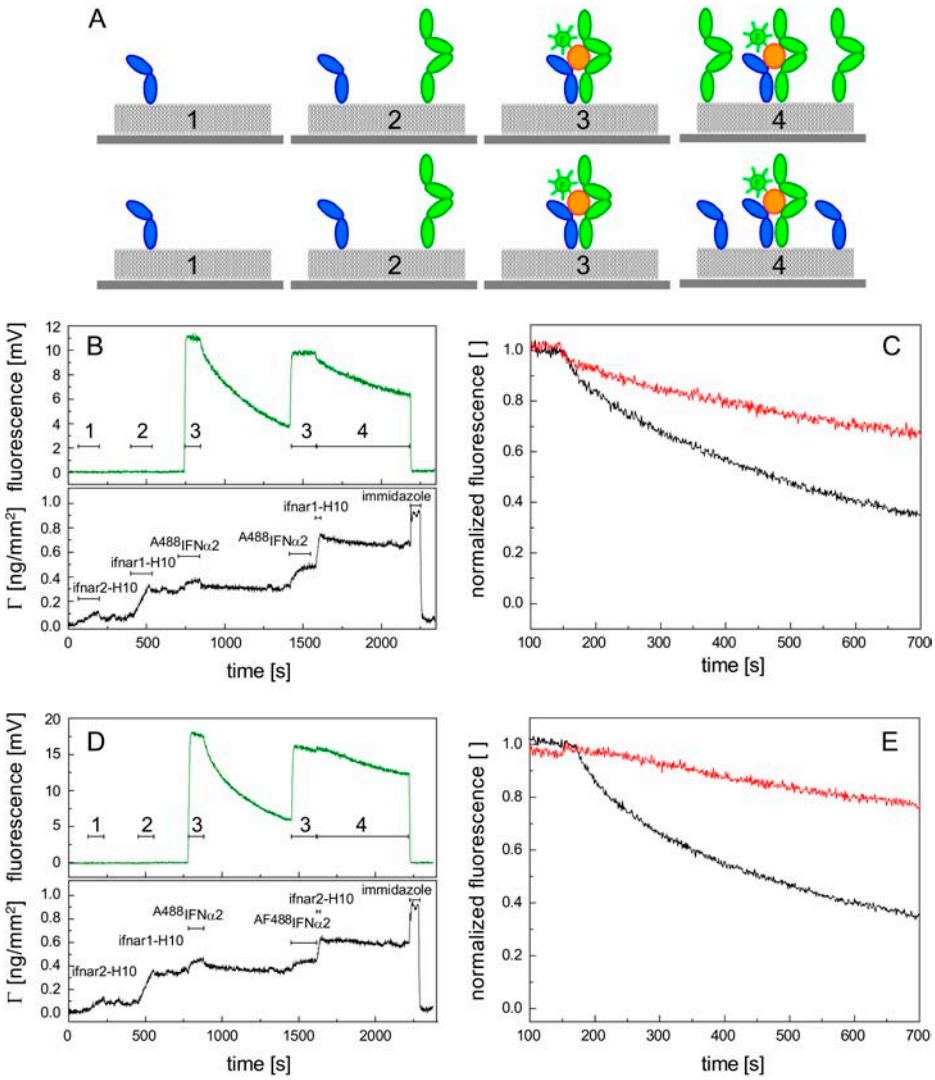

FIGURE 2 Relevance of the two possible dissociation pathways of the ternary complex. (*A*) Schematic of the experiments: ternary complex on fluid lipid membrane was formed by sequential tethering of (2 fmol/mm^2) ifnar2-H10 (*1*) and (3 fmol/mm^2) ifnar1-H10 (*2*) in stoichiometric amounts, followed by binding ^{AF488}IFNα2 to form the ternary complex (*3*). After the second injection of ^{AF488}IFNα2, additional ifnar1-H10 (*top*) or ifnar2-H10 (*bottom*) was rapidly tethered onto the membrane, and dissociation was monitored (*4*). (*B*) Course of a typical experiment as monitored by simultaneous TIRFS (*top*) and RIf (*bottom*) detection with addition loading of (4 fmol/mm^2) ifnar1-H10. (*C*) Overlay of ligand dissociation curves with (*red*) and without (*black*) free ifnar1-H10 on the membrane. (*D*) Course of a typical experiment as monitored by simultaneous TIRFS (*top*) and RIf (*bottom*) detection with additional loading of (7 fmol/mm^2) ifnar2-H10. (*E*) Overlay of ligand dissociation curves with (*red*) and without (*black*) free ifnar2-H10 on the membrane.

to the low affinity of wild-type IFNα2 to ifnar1-H10 and its fast dissociation from ifnar1-H10 (k_d: $\sim$1 s^{-1}). By injection of 1 μM unlabeled IFNα2 HEQ, which binds to ifnar1-H10 with 20-fold higher affinity (27), these free ifnar1-EC molecules are rapidly saturated with ligand. The labeled ligand in the ternary complex is first exchanged against unlabeled IFNα2 HEQ by two-dimensional dissociation of the ifnar2-H10/IFNα2 interaction, followed by dissociation from excess ifnar1-H10 into solution (see Fig. 4 *A*). Because of the fast dissociation of labeled IFNα2 from excess ifnar1-H10 into solution, the rate-limiting step of this exchange process is the dissociation of the ifnar1-H10/IFNα2 complex from ifnar2-H10, which is again the two-dimensional dissociation rate constant k_{-3}. A typical course of such an experiment is shown in Fig. 4 *B*. After tethering the receptor subunits in appropriate surface concentrations, ^{AF488}IFNα2 was injected and spontaneous dissociation was monitored. Fast dissociation from excess ifnar1-H10 within a few seconds was followed by very slow dissociation (comparable to the ligand dissociation kinetics in Fig. 2 *A* after loading excess of ifnar1-H10). The same injection of ^{AF488}IFNα2 was repeated, but ligand dissociation was monitored in presence of tag-less ifnar2-EC (ifnar2-tl) to suppress mass-transport dependent rebinding (28,29), which has to be considered at these receptor surface concentrations. After the third injection of ^{AF488}IFNα2, unlabeled IFNα2 HEQ was injected and the exchange kinetics was monitored. Rapid saturation of the excess ifnar1-H10 by binding of IFNα2 HEQ was verified by the RIf signal. The normalized dissociation curves are compared in Fig. 4 *C* with the ligand dissociation from ifnar2-H10 into solution. Again, substantially slower two-dimensional dissociation of ifnar2-H10 from IFNα2 bound to ifnar1-H10 was observed compared to the three-dimensional dissociation. A rate constant k_{-3} of $(0.0044 \pm 0.001)^{s-1}$ was obtained, which is in good agreement with the value obtained by pulse-chasing with ifnar2-H10.

From the spontaneous ligand dissociation kinetics, the two-dimensional association rate constant was determined, assuming that dissociation through pathway 1 can be neglected

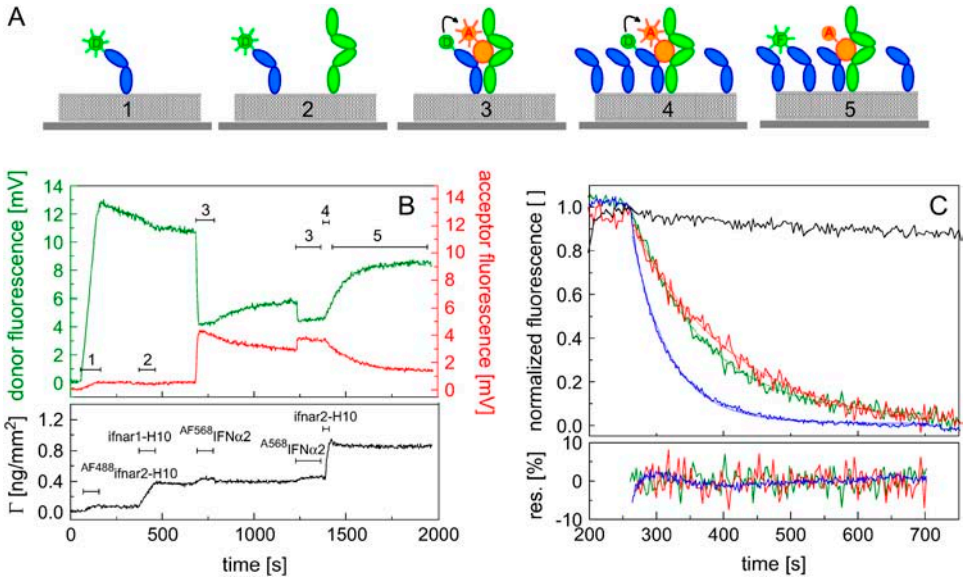

FIGURE 3 Monitoring two-dimensional dissociation kinetics by pulse-chasing the ternary complex. (*A*) Principle of surface-dissociation rate-constant determination as detected by FRET: The ternary complex on fluid lipid membrane is formed by sequential injection of ^{AF488}ifnar2-H10 (*1*), ifnar1-H10 (*2*), and ^{AF568}IFNα2 (*3*). Equilibrium is then perturbed by rapidly tethering an excess of nonlabeled ifnar2-H10 onto the membrane (*4*), which exchanges the labeled ifnar2-H10 in the ternary complex (*5*). (*B*) Course of a typical experiment monitoring donor fluorescence (*green*) and acceptor (*red trace*) fluorescence by TIRFS and the mass loading by RIf (*black*) (2 fmol/mm^2 ^{AF488}ifnar2-H10, 5 fmol/mm^2 ifnar1-H10, 16 fmol/mm^2 ifnar2-H10). (*C*) Comparison of the surface dissociation rates from donor (*green*) and acceptor (*red*) channels with the dissociation of ^{AF568}IFNα2 from ifnar2-H10 alone (*blue*). A control experiment carried out the same way, but with unlabeled ifnar2-H10 in *1* and with direct excitation of ^{AF568}IFNα2 confirmed negligible ligand dissociation from the surface (*black*). The residuals from monoexponential curve fits are shown in the bottom.

at this high excess of ifnar1-EC. Since spontaneous dissociation was indeed biased by rebinding (Fig. 4 *C*), the dissociation curve in presence of 2 μM ifnar2-tl was used. A two-step dissociation model (Eq. 3) was fitted taking into account the appropriate two- and three-dimensional rate constants k_{-3} and k_{-4}, respectively, as well as the surface concentration of ifnar2-H10 as quantified from the RIf signal. A two-dimensional association rate constant k_3 of 3.3×10^{16} mm^2 mol^{-1} s^{-1} was obtained from the fit. Thus, a two-dimensional equilibrium dissociation constant (K_3) of 0.004 fmol/mm^2 or 2.3 molecules/μm^2 was obtained for the IFNα2/ifnar2 interaction.

The same experiment was carried out with the ifnar2-H10 mutant I47A, which binds IFNα2 with 20-fold lower affinity, but with the same association rate constant. Much faster spontaneous ligand dissociation from the ternary complex was observed at similar receptor surface concentrations used for wt ifnar2-H10 (Fig. 4 *D*). Upon chasing with IFNα2 HEQ, the labeled ligand was exchanged within a few 10 seconds. Comparison of two- and three-dimensional dissociation kinetics (Fig. 4 *E*), however, again yielded an approximately threefold lower rate constant for the interaction in plane of the membrane ($k_{-3} = 0.11$ s^{-1}) compared to the dissociation of the ligand from the surface ($k_{-1} = 0.35$ s^{-1}). In contrast, the two-dimensional association rate constant k_{-3} obtained from fitting the spontaneous dissociation kinetics with a two-step dissociation model (Eq. 3) was 2.8×10^{16} mm^2 mol^{-1} s^{-1}, i.e., very similar to the k_3 obtained for the interaction of IFNα2 with wild-type ifnar2-H10 interaction. These consistent results confirmed that the surface-dissociation kinetics is affected by tethering the receptor subunits to the membrane, and the robustness of the experimental approach to determine two-dimensional rate constants.

The two-dimensional interaction involved in pathway 2 was furthermore characterized by applying the IFNα2 mutant R144A (data not shown), which binds ifnar2-H10 with a 10-fold lower association rate constant than wild-type IFNα2 (see Table 1). Again, approximately three-times slower dissociation in plane of the membrane ($k_{-3} = 0.012$ s^{-1}) was observed compared to the dissociation from the surface ($k_{-1} = 0.044$ s^{-1}). More importantly, however, a slower two-dimensional association rate constant ($k_3 = 9.1 \times 10^{15}$ mm^2 mol^{-1} s^{-1}) was obtained, which was approximately threefold slower than the two-dimensional association rate constant of wild-type IFNα2. Thus, the 10-fold difference of the k_a in solution was not maintained on the membrane surface, suggesting that the slower diffusion on the membrane may affect association kinetics.

The two-dimensional rate constants of pathway 1

To determine the two-dimensional rate constants of the interaction between ifnar1-H10 and IFNα2 in the ternary complex we studied the ligand dissociation pathway 1 by a similar set of experiments. To ensure that two-dimensional dissociation is rate-limiting, ifnar2-H10 I47A was used in combination with IFNα2 HEQ, which dissociates from ifnar1-EC with a rate constant of 0.05 s^{-1}. The ligand chasing experiment were carried out at an excess of ifnar2-H10 I47A, and wild-type IFNα2 was used for chasing (Fig. 5 *A*). A typical experiment is shown Fig. 5 *B*: After formation of the ternary complex with ^{AF488}IFNα2 HEQ, spontaneous dissociation was monitored in presence of 2 μM ifnar2-tl to

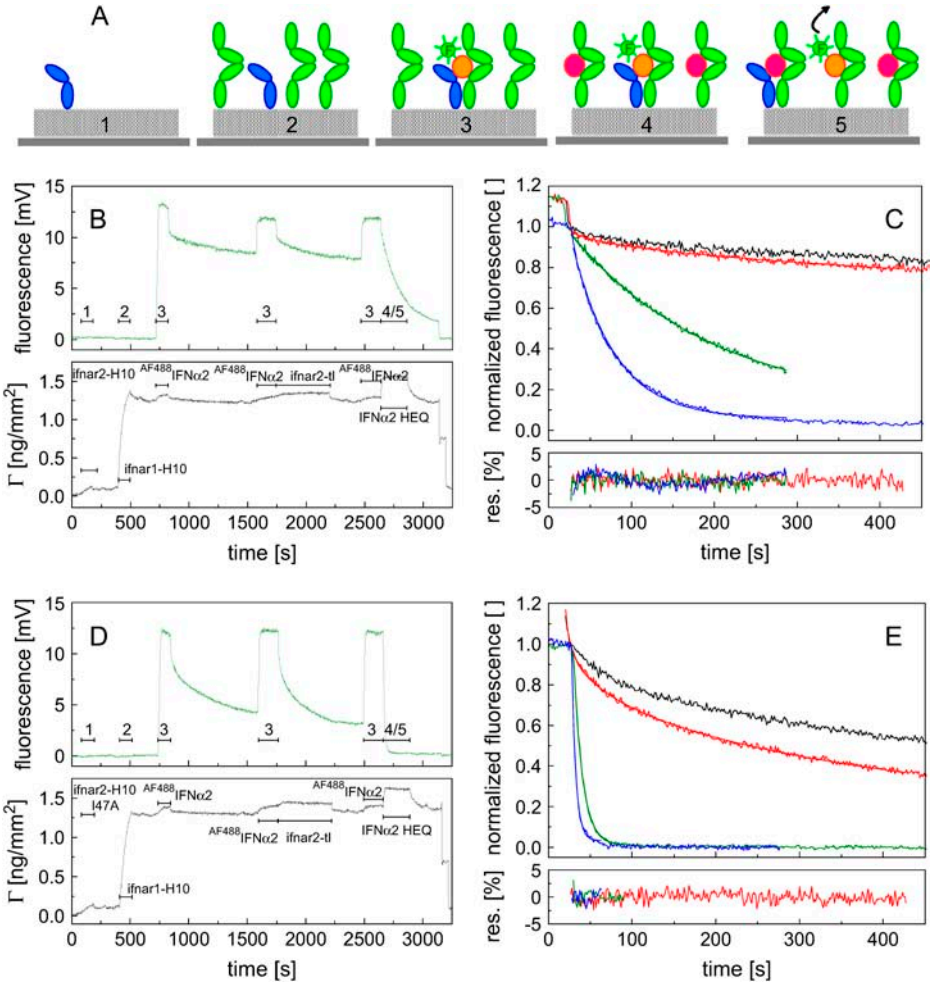

FIGURE 4 Determination of two-dimensional dissociation rate constants by ligand chasing. (*A*) Schematic of the assay: Ternary complex on fluid lipid membrane was formed by sequential injection of ifnar2-H10 (*1*), a large excess of ifnar1-H10 (*2*), and ^{AF488}IFNα2 (*3*). The excess of ifnar1 was then loaded with an unlabeled competitor (*4*), which binds ifnar1 with high affinity (IFNα2 HEQ) and exchanged the labeled ligand in the ternary complex (*5*). (*B*) Typical experiment carried out with the wild-type proteins as detected by TIRFS (*green*) and by RIf (*black*) (2 fmol/mm^2 ifnar2-H10, 20 fmol/mm^2 ifnar1-H10). After the second injection of ^{AF488}IFNα2, 2 μM ifnar2-tl was injected to eliminate rebinding. After the third injection of ^{AF488}IFNα2, 1 μM unlabeled IFNα2 HEQ was injected. (*C*) Overlay of the normalized ^{AF488}IFNα2 dissociation curves from panel *B*: spontaneous dissociation during washing with buffer (*black*) and with 2 μM ifnar2-tl (*red*), as well as dissociation while chasing with IFNα2 HEQ (*green*). Dissociation from ifnar2-H10 alone is shown for comparison (*blue*). The residuals from the curve fits are shown in the bottom. (*D*) Same experiment as in panel *B* carried out with ifnar2-H10 I47A (2 fmol/mm^2 ifnar2-H10 I47A, 20 fmol/mm^2 ifnar1-H10). (*E*) Overlay of the dissociation curves from panel *D* (same color-coding as in panel *C*) with comparison of ^{AF488}IFNα2 dissociation from ifnar2-H10 I47A alone (*blue*). The residuals from the curve fits are shown in the bottom.

suppress rebinding of the ligand. After a second injection of ^{AF488}IFNα2 HEQ, ligand exchange in presence of unlabeled wild-type IFNα2 was monitored. In Fig. 5 *C*, the dissociation kinetics in plane of the membrane is compared with the dissociation from the surface. Again, significantly lower dissociation rate constant was obtained for two-dimensional dissociation (k_{-2}: 0.026 s^{-1}) was observed compared to the dissociation into solution (k_{-4}: 0.047 s^{-1}). Based on this two-dimensional dissociation rate constant, the spontaneous ligand dissociation kinetics was fitted by a two-step model (Eq. 2). A two-dimensional association rate constant of 1.3 $\times$ 10^{16} mm^2 mol^{-1} s^{-1} was obtained for the interaction of IFNα2 HEQ with ifnar1-H10 (k_2). These measurements were also carried out with different combinations of wild-type and mutant IFNα2 and ifnar2-H10. All results are summarized in Table 2. In all combinations, similar values of $\sim$1 $\times$ 10^{16} mm^2 mol^{-1} s^{-1} were obtained for k_2, very similar to the k_3 obtained for IFNα2 R144A. Interestingly, also the three-dimensional association rate constants k_1 and k_4 are very similar for this mutant (see Table 1). Furthermore, an $\sim$2.5-fold lower k_{-2} compared to k_2 was confirmed for all combinations, confirming the decrease in the dissociation rate constant by tethering the complex onto the surface. Based on these consistent observations, we estimated a k_{-2} of 0.4 s^{-1} for wild-type IFNα2.

The role of orientation in two-dimensional interactions

Orientation and flexibility of membrane-anchored proteins have been suggested to be key parameters in the kinetics of two-dimensional interactions on membranes. To study the role of orientation on ternary complex formation, we tethered ifnar1-EC through an N-terminal decahistidine tag (H10-ifnar1) onto the membrane. For this protein, very similar rate constants as for ifnar1-H10 were obtained by conventional ligand binding assays (Table 1). The two-dimensional rate constants were determined using ligand chasing experiments, as described above. The results are summarized in Table 2. No significant effect on the surface dissociation rate constants $k-_2$ and $k-_3$ was observed upon changing the orientation of ifnar1-EC. The effect on the two-dimensional association rate constants, however, was substantial: for k_2 (pathway 1), an approximately-threefold decrease was

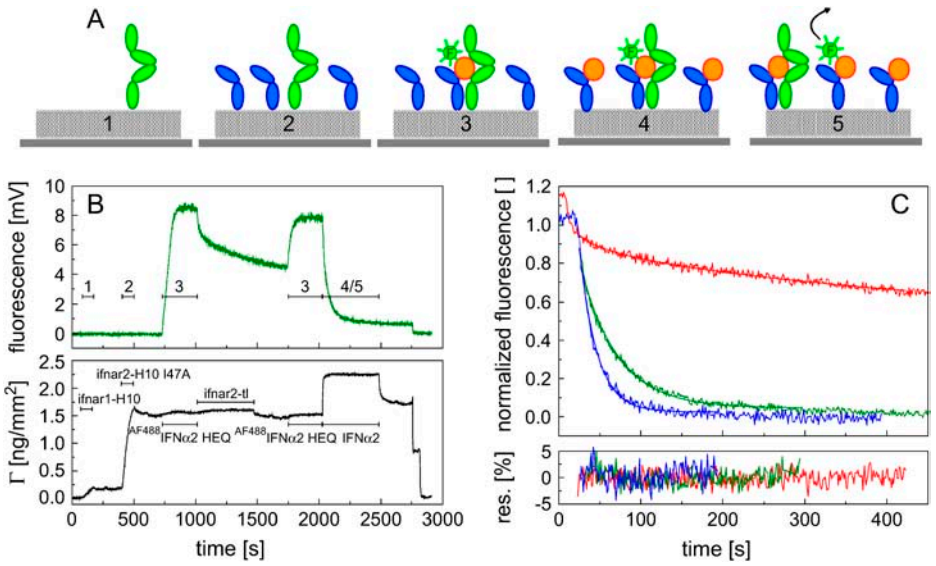

FIGURE 5 Determination of two-dimensional rate constants for pathway 1. (*A*) Schematic of the assay: ternary complex on fluid lipid membrane was formed by sequential injection of ifnar1-H10 (*1*), excess ifnar2-H10 I47A (*2*), and ^{AF488}IFNα2 HEQ (*3*). Upon loading the excess binding sites of ifnar2-H10 with unlabeled IFNα2 (*4*), labeled IFNα2 in the ternary complex was exchanged (*5*). (*B*) Course of a typical experiment as detected by TIRFS (*green*) and RIf (*black*). During spontaneous ligand dissociation, 2 μM ifnar2-tl was maintained in the background to eliminate rebinding. After the second injection of ^{AF488}IFNα2 HEQ 1 μM unlabeled IFNα2-wild-type was injected (2.5 fmol/mm^2 ifnar1-H10, 50 fmol/mm^2 ifnar2-H10 I47A). (*C*) Overlay of the normalized dissociation curves: spontaneous dissociation from the ternary complex (*red*) and ligand exchange kinetics washing with 1 μM IFNα2 HEQ (*green*). Dissociation from Ifnar1-H10 alone is shown for comparison (*blue*). The residuals from the curve fits are shown in the bottom.

observed compared to the rate constant obtained with ifnar1-H10. For k_3 (pathway 2), the effect was even stronger with an approximately-fivefold decrease compared to the rate constant obtained with ifnar1-H10. Thus, we could demonstrate the key role of receptor orientation on surface association kinetics and affinity by mimicking oriented attachment to the membrane in vitro.

Population of the dissociation pathways

Based on the experimentally determined rate constants, the population of the two dissociation pathways was compared at experimentally relevant receptor surface concentrations by numerically simulating ligand dissociation (Eq. 4). The ligand dissociation curves for both pathways together and individually are compared for the wild-type proteins and two mutants in Fig. 6. At stoichiometric concentration of the receptor subunits, pathway 1 is clearly dominant in the case of the wt proteins (Fig. 6 *A*), and also for ifnar2-I47A (Fig. 6 *B*). However, a substantial contribution of pathway 2 to ligand dissociation is observed, which is in line with the only approximately-threefold-higher two-dimensional association rate k_3 compared to k_2. For IFNα2 R144A ($k_3 \approx k_2$), both pathways are similarly populated at stoichiometric receptor concentrations, confirming the key role of the relative surface two-dimensional association rate constants on the dissociation pathway. At 10-fold excess of ifnar2 or ifnar1, only pathway 1 or pathway 2, respectively, is responsible for ligand dissociation.

TABLE 2 Two-dimensional interaction rate constants determined for different combinations of receptor and ligand variants

Ifnar2-H10/IFNα2/ifnar1-EC	Pathway 1			Pathway 2			Balance
	k_2 [mm^2 fmol^{-1} s^{-1}]	k_{-2} [s^{-1}]	K_2 [fmol/mm^2]	k_3 [mm^2 fmol^{-1} s^{-1}]	k_{-3} [s^{-1}]	K_3 [fmol/mm^2]	$\frac{K_1 \times K_2}{K_3 \times K_4}$
I47A/wt/C-term*	16.5 ± 3.3	~0.4‡	0.024	28.2 ± 5.1	0.11 ± 0.02	0.004	0.2
I47A/R144A/C-term*	9.6 ± 2.0	~0.4‡	0.042	11.3 ± 2.2	0.2 ± 0.02	0.018	0.79
wt/R144A/C-term*	9.1 ± 1.8	~0.4‡	0.044	9.1 ± 2.0	0.012 ± 0.001	0.0013	1.02
wt/wt/C-term*			0.024	33 ± 5.5	0.0044 ± 0.001	0.00013	0.26
wt/HEQ/C-term*					0.004		
I47A/HEQ/C-term*	13.1 ± 2.8	0.026 ± 0.002	0.002			0.004	0.3
wt/wt/N-term†			0.1	5.2 ± 1.2	0.007 ± 0.002	0.0014	0.1
I47A/wt/N-term†	4.0 ± 0.8	~0.4‡	0.100	5.0 ± 1.0	0.070 ± 0.005	0.014	0.21
I47A/HEQ/N-term†	4.0 ± 0.9	0.033 ± 0.004	0.008			0.014	0.34

*ifnar1-EC tethered to the membrane by a C-terminal H10-tag.
†ifnar1-EC tethered to the membrane by a N-terminal H10-tag.
‡Estimated by comparison with IFNα2 HEQ.

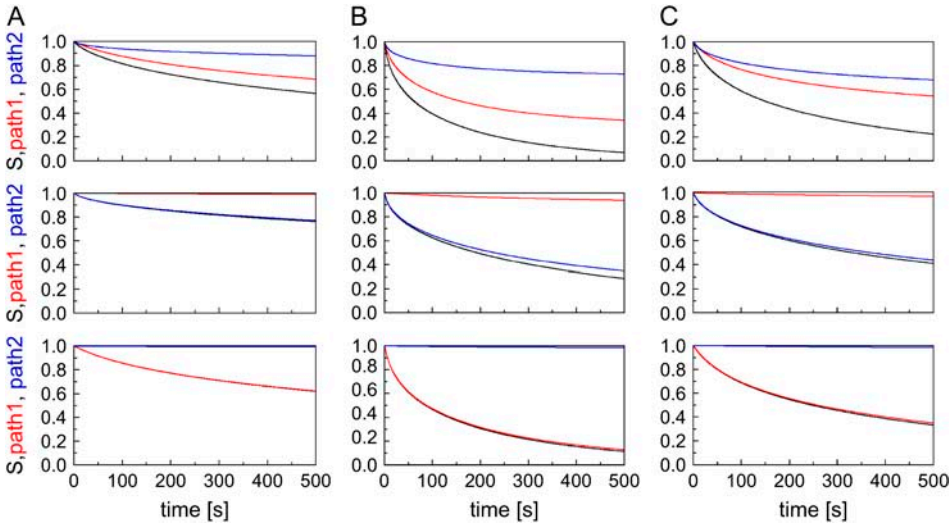

FIGURE 6 Population of the dissociation pathways under different conditions. Ligand dissociation was numerically simulated based on the experimentally determined two- and three-dimensional rate constants for the following species of ifnar2/IFNα2/ifnar1: wt/wt/wt (*A*); I47 A/wt/wt (*B*); and wt/R144A/wt (*C*). In all cases, 2 fmol/mm^2 of both ifnar2 and ifnar1 were assumed to form ternary complex under three different condition: no excess of either of the receptor subunits (*top panel*), with an excess of 20 fmol/mm^2 ifnar1 (*middle panel*), and with an excess of 20 fmol/mm^2 ifnar2 (*bottom panel*).

DISCUSSION

Cellular signaling by cytokine receptors is initiated by ligand-mediated cross-linking of two or more receptor subunits. Thus, the two-dimensional interactions between the ligand and its cognate receptor subunits determine the dynamics of the receptor complex on the plasma membrane, which has been proposed to play a critical role for signaling and its regulation. Here, we have for the first time, to our knowledge, parameterized the rate constants of a ternary cytokine-receptor complex on model membranes. By exchange experiments based on chasing the ternary complex with additional receptor or ligand, we succeeded in reliably determining the two-dimensional dissociation rate constants. The two possible pathways were studied separately by using excess concentrations of one of the receptor subunits. Based on several mutants and variants of the interacting proteins, the effect of different rate constants and protein orientation on the complex dynamics was studied. Thus, we have identified several critical features of two-dimensional interactions on membranes, which cannot be readily concluded from solution-binding assays. The first surprising observation was that the dissociation rate constants were generally two-to-threefold lower for the interaction in plane of the membrane compared to the interaction in solution. This difference was not due to cooperative binding of the receptor subunits, which was confirmed by extensive ligand binding studies. Surface anchoring limits the degree of freedom, which may affect the reaction coordinate, but the dissociation kinetics in plane of the membrane was hardly significantly affected by the orientation of ifnar1-EC. The environment of the interaction interface is not affected by membrane anchoring, but the separation of the interaction partners by lateral diffusion, is ~100-fold slower on the membrane than in solution, which may account for the slower dissociation. Furthermore, more efficient rebinding of the membrane-anchored proteins before full dissociation may be caused by reducing rotational freedom. The first explanation implies that the dynamics of ligand-receptor complexes may depend on the diffusion properties of the receptor in the membrane, which are known to be locally rather variable due to the microdomain structure of the plasma membrane. By partitioning of receptor complexes in microdomains with low fluidity such as caveolae, which has been reported for several tyrosine kinases and cytokine receptors (30,31) including ifnar (32), the stability of oligomeric complexes would be substantially enhanced. This could be a simple mechanism for increasing receptor recruitment efficiency at low receptor surface concentration. However, more detailed analysis of the dependence of the two-dimensional k_d on membrane fluidity would be required, as well as confirmation for other ligand-receptor complexes.

Assessment of the association rate constants in plane of the membrane and toward the receptor subunits revealed further striking features of interactions on membranes. More than 10-fold faster association of IFNα2 with ifnar2 compared to ifnar1-EC suggested that pathway 1 dominates both formation and dissociation of the ternary complex. On the membrane, though, a less-than-threefold difference in the two-dimensional association rate constants was observed. For the IFNα2 mutant R144A, which binds to ifnar2-EC with a 10-fold lower association rate constant than wild-type IFNα2, similar two-dimensional association rate constants were obtained for both pathways. It was shown earlier that the association kinetics of IFNα2 to ifnar2 is accelerated by electrostatic attraction (20). Electrostatic association rate enhancement has been explained by a stabilization of the encounter complex and by steering of the proteins into appropriate orientations (33–36). Our results suggest that this electrostatic rate enhancement is not as effective on the membrane. This could be ascribed to changed electrostatic

properties by tethering the interacting proteins onto the membrane. Another reason could be that the association kinetics is limited by the slower diffusion on the membrane. While electrostatic steering did not seem to be as important as in solution, receptor orientation was shown to strongly affect the two-dimensional association rate constants. Interestingly, even more similar values were observed for both k_2 and k_3 upon tethering ifnar1-EC through the N-terminus. Compared to the rate constants obtained with ifnar1-EC tethered in its natural orientation, both k_2 and k_3 were substantially decreased. Orientation has been proposed to play a key role for two-dimensional interactions on membranes (37); the strong effect, though, is somewhat surprising because tethering through the histidine tag to the membrane is expected to provide substantial flexibility, which should counteract preorientation. Furthermore, ifnar1-EC comprising four Ig-like domains is probably rather flexible in itself. However, our results suggest that steering of association by oriented anchoring in the membrane is more critical for two-dimensional association kinetics than electrostatic steering. We have shown here that membrane anchoring through histidines can in principle mimic some determinant of ligand-receptor interaction on membranes. The importance of lateral diffusion kinetics, orientation, and flexibility underscore the importance of assessing transmembrane proteins interactions under conditions, which mimic the properties of membrane anchoring even more appropriately.

We thank Dr. Suman Lata for providing *bis*-NTA lipid and for stimulating discussions. The hospitality and the support from the laboratory of Robert Tampé are gratefully acknowledged. The plasmid for expression of IFNα2 HEQ was obtained from Dr. Gideon Schreiber, Rehovot.

This project was supported by the Deutsche Forschungsgemeinschaft (grants No. Pi 405/1, No. Pi 405/2, and No. SFB 628), and by the Human Frontier Science Program (grant No. RGP60/2002).

REFERENCES

1. Schlessinger, J. 1988. Signal transduction by allosteric receptor oligomerization. *Trends Biochem. Sci.* 13:443–447.
2. Ullrich, A., and J. Schlessinger. 1990. Signal transduction by receptors with tyrosine kinase activity. *Cell.* 61:203–212.
3. Cunningham, B. C., M. Ultsch, A. M. De Vos, M. G. Mulkerrin, K. R. Clauser, and J. A. Wells. 1991. Dimerization of the extracellular domain of the human growth hormone receptor by a single hormone molecule. *Science.* 254:821–825.
4. Whitty, A., N. Raskin, D. L. Olson, C. W. Borysenko, C. M. Ambrose, C. D. Benjamin, and L. C. Burkly. 1998. Interaction affinity between cytokine receptor components on the cell surface. *Proc. Natl. Acad. Sci. USA.* 95:13165–13170.
5. Schlessinger, J. 2000. Cell signaling by receptor tyrosine kinases. *Cell.* 103:211–225.
6. Sebald, W., and T. D. Mueller. 2003. The interaction of BMP-7 and ActRII implicates a new mode of receptor assembly. *Trends Biochem. Sci.* 28:518–521.
7. Stroud, R. M., and J. A. Wells. 2004. Mechanistic diversity of cytokine receptor signaling across cell membranes. *Sci. STKE.* 2004:re7.
8. DeLisi, C., and R. Chabay. 1979. The influence of cell surface receptor clustering on the thermodynamics of ligand binding and the kinetics of its dissociation. *Cell Biophys.* 1:117–131.
9. DeLisi, C. 1981. The effect of cell size and receptor density on ligand-receptor reaction rate constants. *Mol. Immunol.* 18:507–511.
10. McCloskey, M. A., and M. M. Poo. 1986. Rates of membrane-associated reactions: reduction of dimensionality revisited. *J. Cell Biol.* 102:88–96.
11. Axelrod, D., and M. D. Wang. 1994. Reduction-of-dimensionality kinetics at reaction-limited cell surface receptors. *Biophys. J.* 66:588–600.
12. Kholodenko, B. N., J. B. Hoek, and H. V. Westerhoff. 2000. Why cytoplasmic signalling proteins should be recruited to cell membranes. *Trends Cell Biol.* 10:173–178.
13. Perelson, A. S., and C. Delisi. 1980. Receptor clustering on a cell-surface. 1. Theory of receptor cross-linking by ligands bearing two chemically identical functional groups. *Math. Biosci.* 48:71–110.
14. Adam, G., and M. Delbruck. 1968. Reduction of dimensionality in biological diffusion processes. *In* Structural Chemistry and Molecular Biology. A. Rich and N. Davidson, editors. W.H. Freeman, New York. 198–215.
15. Dustin, M. L., L. M. Ferguson, P. Y. Chan, T. A. Springer, and D. E. Golan. 1996. Visualization of CD2 interaction with LFA-3 and determination of the two-dimensional dissociation constant for adhesion receptors in a contact area. *J. Cell Biol.* 132:465–474.
16. Yang, T., O. K. Baryshnikova, H. Mao, M. A. Holden, and P. S. Cremer. 2003. Investigations of bivalent antibody binding on fluid-supported phospholipid membranes: the effect of hapten density. *J. Am. Chem. Soc.* 125:4779–4784.
17. Lata, S., M. Gavutis, and J. Piehler. 2006. Monitoring the dynamics of ligand-receptor complexes on model membranes. *J. Am. Chem. Soc.* 128:6–7.
18. Lamken, P., S. Lata, M. Gavutis, and J. Piehler. 2004. Ligand-induced assembling of the type I interferon receptor on supported lipid bilayers. *J. Mol. Biol.* 341:303–318.
19. Gavutis, M., S. Lata, P. Lamken, P. Müller, and J. Piehler. 2005. Lateral ligand-receptor interactions on membranes probed by simultaneous fluorescence-interference detection. *Biophys. J.* 88:4289–4302.
20. Piehler, J., and G. Schreiber. 1999. Biophysical analysis of the interaction of human ifnar2 expressed in *E. coli* with IFN α2. *J. Mol. Biol.* 289:57–67.
21. Lamken, P., M. Gavutis, I. Peters, J. Van der Heyden, G. Uze, and J. Piehler. 2005. Functional cartography of the extracellular domain of the type I interferon receptor subunit ifnar1. *J. Mol. Biol.* 350:476–488.
22. Piehler, J., and G. Schreiber. 2001. Fast transient cytokine-receptor interactions monitored in real time by reflectometric interference spectroscopy. *Anal. Biochem.* 289:173–186.
23. Goldstein, B., D. Coombs, X. He, A. R. Pineda, and C. Wofsy. 1999. The influence of transport on the kinetics of binding to surface receptors: application to cells and BIAcore. *J. Mol. Recog.* 12:293–299.
24. Piehler, J., L. C. Roisman, and G. Schreiber. 2000. New structural and functional aspects of the type I interferon-receptor interaction revealed by comprehensive mutational analysis of the binding interface. *J. Biol. Chem.* 275:40425–40433.
25. Piehler, J., and G. Schreiber. 1999. Mutational and structural analysis of the binding interface between type I interferons and their receptor ifnar2. *J. Mol. Biol.* 294:223–237.
26. Roisman, L. C., D. Jaitin, D. P. Baker, and G. Schreiber. 2005. Mutational analysis of the IFNAR1 binding site on IFNα2 reveals the architecture of a weak ligand-receptor binding-site. *J. Mol. Biol.* 353:271–281.
27. Jaitin, D., L. C. Roisman, E. Jaks, M. Gavutis, J. Piehler, J. Van der Heyden, G. Uze, and G. Schreiber. 2006. Inquiring into the differential actions of interferons: an IFNa2 mutant endowed with enhanced

binding affinity to IFNAR1 is functionally similar to IFNβ. *Mol. Cell. Biol.* 26:1888–1897.

28. Schuck, P., and A. P. Minton. 1996. Analysis of mass transport-limited binding kinetics in evanescent wave biosensors. *Anal. Biochem.* 240: 262–272.
29. Schuck, P. 1996. Kinetics of ligand binding to receptor immobilized in a polymer matrix, as detected with an evanescent wave biosensor. I. A computer simulation of the influence of mass transport. *Biophys. J.* 70:1230–1249.
30. Le Roy, C., and J. L. Wrana. 2005. Clathrin- and non-clathrin-mediated endocytic regulation of cell signalling. *Nat. Rev. Mol. Cell Biol.* 6: 112–126.
31. Rao, R., B. Logan, K. Forrest, T. L. Roszman, and J. Goebel. 2004. Lipid rafts in cytokine signaling. *Cytokine Growth Factor Rev.* 15:103–110.
32. Takaoka, A., Y. Mitani, H. Suemori, M. Sato, T. Yokochi, S. Noguchi, N. Tanaka, and T. Taniguchi. 2000. Cross talk between interferon-γ and -α/β-signaling components in caveolar membrane domains. *Science.* 288:2357–2360.
33. Schreiber, G., and A. R. Fersht. 1996. Rapid, electrostatically assisted association of proteins. *Nat. Struct. Biol.* 3:427–431.
34. Sheinerman, F. B., R. Norel, and B. Honig. 2000. Electrostatic aspects of protein-protein interactions. *Curr. Opin. Struct. Biol.* 10:153–159.
35. Selzer, T., and G. Schreiber. 2001. New insights into the mechanism of protein-protein association. *Proteins.* 45:190–198.
36. Schreiber, G. 2002. Kinetic studies of protein-protein interactions. *Curr. Opin. Struct. Biol.* 12:41–47.
37. Berg, O. G. 1985. Orientation constraints in diffusion-limited macromolecular association. The role of surface diffusion as a rate-enhancing mechanism. *Biophys. J.* 47:1–14.